Improving Nonenzymatic Biosensing Performance of Electrospun Carbon Nanofibers Decorated With Ni/Co Particles via Oxidation

Ali Mohammadpour-Haratbar
Amirkabir University of Technology
Saeedeh Mazinani (s.mazinani@aut.ac.ir)
Amirkabir University of Technology https://orcid.org/0000-0003-2778-4602
Farhad Sharif
Amirkabir University of Technology
Ali Mohammad Bazargan
Amirkabir University of Technology

Research Article

Keywords: Non-enzymatic biosensors, 2D materials, Ni/Co hybrid nanostructure

Posted Date: October 13th, 2021

DOI: https://doi.org/10.21203/rs.3.rs-856269/v1

Version of Record: A version of this preprint was published at Applied Biochemistry and Biotechnology on February 16th, 2022. See the published version at https://doi.org/10.1007/s12010-022-03833-8.

Abstract

Electrochemical nonenzymatic biosensors with no immobilization and degradation problem, have recently attracted growing attention due to stability and reproducibility. Here, a comparative study was conducted to precisely evaluate the nonenzymatic glucose sensing of pure/oxidized Ni, Co, and their bimetal nanostructures grown on electrospun carbon nanofibers (ECNFs). This method provides a low-cost free stand electrode. The prepared nanostructures with superb physiochemical features exhibited sensitivity (from 66.28 to 610.6 μA mM^{-1} cm^{-2}), linear range of 2-10 mM, limit of detection in the range of 1 mM, and response time (<5 s), besides outstanding selectivity and applicability for glucose detection in the human serum. Regarding Co-C and Ni-C phase diagrams, solid-state diffusion phenomena, and rearrangement of dissolved C atoms after migration from metal particles was discussed. This study undoubtedly provides new prospects on nonenzymatic biosensing performance of mono-metal, bimetal, and oxide compounds of Ni and Co elements, which is useful for the fabrication of biomolecules detecting devices.

1. Introduction

Electrochemical biosensors are a major group of biosensors including considerable applications due to their high sensitivity, ease of construction, and low cost [1,2]. These biosensors are categorized into two types of enzymatic and nonenzymatic. Enzymatic biosensors have advantages such as excellent selectivity, fast performance, and good catalytic activity, all of which improve the sensitivity of the sensor [3]. Despite the stated merits, recent research has often focused on enzyme-free biosensors due to the complexity of the enzyme immobilization method, thermal and chemical instability, high expense of enzymes, and the dependence of sensor sensitivity on temperature, pH, and humidity [4].

One of the essential parameters in the performance of biosensors is the sensitivity of the electrode employed in the design of the sensor. In recent years, electrodes of carbon-based nanomaterials such as carbon nanotubes, graphene, and carbon nanofibers (CNFs) have been applied as substrates and protectors to increase the electrical conductivity of biosensor electrodes [5–7]. The presence of conductive carbon nanomaterials accompanied with a very high specific surface area facilitates charge transfer and rapid electron transfer, which in turn increases the sensitivity of biosensor [8,9].

Among carbon materials, carbon nanofibers as one-dimensional carbon nanomaterials and carbon-nanofibers-based nanocomposites have recently been used in supercapacitors [10], fuel cells [11], catalyst protectors [12], and gas sensors [13]. Since they can be employed simultaneously both as a transducer which relays the electrochemical signal and as a highly porous matrix for further loading of nanoparticles. Furthermore, compared to other carbon nanomaterials, carbon nanofibers can be used directly as an electrode without any binders, which increases the electrical conductivity of the electrodes [14].

Recently, electrospinning has been recognized as a simple and economical technique for making one-dimensional polymer-based ECNFs with diameters ranging from tens nanometers to several microns [15]. Among the various precursors employed to produce ECNFs, polyacrylonitrile (PAN) has been used as a common polymer due to its easy carbonization process and high carbon yield [16]. The electrospinning process can also be utilized to prepare metallic nanoparticles (N.P.s) / ECNF composites. This can be done by spinning PAN nanofibers containing metal precursors and subsequently a heat treatment process for electrocatalytic applications. NPs / ECNF composites, prepared through electrospinning method, enjoy high mechanical strength, and the N.P.s are uniformly dispersed in and on the surface of ECNFs [17]. The presence of metal N.P.s can increase the arrangement of fibers in ECNF and the degree of ECNF graphitization. Among the transition metals, elements such as nickel (Ni), iron (Fe), cobalt (Co), platinum (Pt), molybdenum (Mo), chromium (Cr), and boron (B) are far effective in catalytic graphitization [18,19]. Furthermore, Ni and Co have displayed superior electrocatalytic properties in biosensor applications. Hence, decorating the pure/oxidized Ni, Co, and their bimetal complex on the surface of ECNFs can be an appropriate candidate in the electrode construction of electrochemical biosensors.

The normal blood glucose concentration range is 3-8 mM [20]. The rise of diabetes has caused concern in the global community and has prompted researchers to carry out research on the development of glucose biosensors with high sensitivity and speed of diagnosis [21]. In order to progress in the nonenzymatic glucose biosensors with high sensitivity and reproducibility, many investigations have been made on different nanomaterials [22]. The electrocatalytic activity toward oxidation of glucose has shown on some noble metals such as Pt and Au. However, these metals are expensive. Furthermore, the surfaces of noble metals are quickly fouling by adsorbed interfering intermediates, and chlorine ions in blood. This causes interference in the sensitivity and performance of biosensors [23]. In order to solve the toxicity problem of noble metals, various transition metals and metal oxides, such as Ni [24], NiO [25], CuO [7], Co3O4 [26] and their alloys, such as Pd–Ni [9], and NiCo2O4 [27] have been investigated in many papers.

In this study, the homogenous PAN solutions with different concentrations of Ni and Co salt precursors were prepared and electrospun to acquire PAN nanofibers and then, they were subjected to stabilization and carbonization heat treatments. Then the resulting nanocomposites were used directly and with no binders in the manufacture of nonenzymatic glucose biosensors as free-standing electrodes. The influence of catalyst content and carbonization time (T_c) parameters on the performances of manufactured biosensors electrode was evaluated.

2. Experimental

2.1. Materials

PAN (average Mw = 80 000, Purchased from Polyacryle co.) was used as the polymer precursor, and N, N-dimethylformamide (DMF, Purchased from Aldrich) was employed as the solvent to prepare the ECNFs matrix solution. Cobalt (II) acetate Tetra hydrate (CoAc, Purchased by Aldrich) and Nickel (II)

acetylacetonate (Ni (acac) $_2$, Purchased from Aldrich) were utilized as the metal precursors of monometal, bimetal and oxide compounds of Ni and Co elements. Glucose, NaOH ascorbic acid (A.A.), uric acid (U.A.), and dopamine (DA) were purchased from Mojallali Industrial Chemical Complex Co. (Iran). All other reagents were of analytical grade and used without further purification. Double distilled water was used for the preparation of all solutions.

2.2. Preparation of pure ECNF

1.2 g of PAN was dissolved in 8.8 g of DMF at room temperature for two hr under magnetic stirring. The mixture was transferred to a plastic capillary and electrospun on a spinning machine (Fanavaran nano-meghyas Co.) with a high voltage at 11.5 kV and the collector-to-needle distance at 10 cm to collect a non-woven mat polymer nanofibers on an aluminum foil fixed collector. Then electrospun nanofibers were stabilized at 230 °C for one hr in an air furnace. Thereafter, stabilized PAN nanofibers were carbonized at 1000 °C for five hr in a nitrogen atmosphere of a tube furnace and pure ECNF was synthesized.

2.3. Preparation of Ni and Ni oxide (NiO) decorated ECNF

In a typical process, 1.2 g of PAN was dissolved in 8.8 g of DMF at room temperature for two hr under magnetic stirring. Then, 0.5 g of Ni (acac) $_2$ was added to the top solution and stirred again for 24 h on the magnetic stirrer. The mixture was transferred to a plastic capillary and electrospun on a spinning machine with a high voltage at 11.5 kV and the collector-to-needle distance at 10 cm. Then electrospun nanofibers were stabilized at 230 °C for one hr in an air furnace. Thereafter, stabilized PAN nanofibers containing Ni salts precursors were carbonized at 1000 °C for five hrs in a nitrogen atmosphere of a tube furnace. Finally, Ni/ ECNF nanocomposites were synthesized. In an effort to identify an optimized composition, different amounts of Ni (acac) $_2$ was added into the fixed amount of PAN precursor, namely, 0.2, 0.35, and 0.5 g, for 1.2 g of PAN. The final products were labeled as 0.2 Ni/ ECNF-5h, 0.35 Ni/ ECNF-5h, and 0.5 Ni/ ECNF-5h, respectively. Also, to identify the optimum T_c, times of 1, 3 and 5 hrs at a constant temperature (1000 °C) and a constant amount of 0.5 g of salt, were selected in a nitrogen gas tube furnace. On the basis of the different T_c, the final products were labeled as 0.5 Ni/ ECNF-1h, 0.5 Ni/ ECNF-3h, and 0.5 Ni/ ECNF-5h.

Furthermore, the carbonized 0.5 Ni/ ECNF-5h was post-heat treated at 300 °C for 15 min in air to precipitate NiO/ ECNF.

2.4. Preparation of Co and Co oxide (Co_3O_4) decorated ECNF

1.2 g of PAN was dissolved in 8.8 g of DMF at room temperature for two hr under magnetic stirring. Then, 0.5 g of CoAc was added to the top solution and stirred again for 24 h on the magnetic stirrer. The mixture was transferred to a plastic capillary and electrospun on a spinning machine with a high voltage at 11.5 kV and the collector-to-needle distance at 10 cm. Then electrospun nanofibers were stabilized at 230 °C for 1 h in an air furnace. Thereafter, stabilized PAN nanofibers containing Co salts precursors were

carbonized at 800 °C for 5 h in a nitrogen atmosphere of a tube furnace. Different amounts of CoAc was added into the fixed amount of PAN precursor, namely, 0.2, 0.35, and 0.5 g, for 1.2 g of PAN to identify an optimized composition, The final products were labeled as 0.2 Co/ ECNF-5h, 0.35 Co/ ECNF-5h, and 0.5 Co/ ECNF-5h, respectively. Besides, Different times of 1, 3 and 5 hr at a constant temperature (800 °C) and a constant amount of 0.5 g of salt, were selected in a nitrogen gas tube furnace to identify the optimum t_c. On the basis of the different t_c, the final products were labeled as 0.5 Co/ ECNF-1h, 0.5 Co/ ECNF-3h, and 0.5 Co/ ECNF-5h.

Furthermore, to precipitate Co_3O_4/ ECNF, the carbonized 0.5 Co/ ECNF-5h was post-heat treated at 300 °C for 15 min in air.

2.5. Preparation of bimetallic Ni/Co decorated ECNF

1.2 g of PAN was dissolved in 8.8 g of DMF at room temperature for 2 hr under magnetic stirring. Then, 0.5 g of Mixture of Ni (acac) $_2$ / CoAc was added to the top solution and stirred again for 24 hr on the magnetic stirrer. The mixture was transferred to a plastic capillary and electrospun on a spinning machine with a high voltage at 11.5 kV and the collector-to-needle distance at 10 cm . Then electrospun nanofibers were stabilized at 230 °C for 1 hr in an air furnace. Thereafter, stabilized PAN nanofibers containing Ni/Co salts precursor were carbonized at 800 °C for 5 h in a nitrogen atmosphere of a tube furnace, respectively. Finally, bimetallic Ni-Co / ECNF nanocomposites were synthesized. In an effort to identify an optimized composition, different ratios of mixture of Ni (acac) $_2$ / CoAc were added into the fixed amount of PAN precursor, namely, 0.05/ 0.45, 0.15/ 0.35, 0.25/ 0.25, 0.35/ 0.15, and 0.45/ 0.05 g for 1.2 g of PAN. The final products were labeled as $Ni_{10}Co_{90}$/ ECNF-5h, $Ni_{30}Co_{70}$/ ECNF-5h, $Ni_{50}Co_{50}$/ ECNF5h, $Ni_{70}Co_{30}$/ ECNF-5h, and $Ni_{90}Co_{10}$/ ECNF-5h, respectively.

Furthermore, in order to precipitate NiCo2O4/ ECNF, the carbonized $Ni_{70}Co_{30}$/ ECNF-5h was post-heat treated at 300 °C for 15 min in air.

Higher amounts of CoAc or Ni (acac) $_2$ resulted in difficulties in electrospinning; thus, no further attempts were made to increase the metal precursor's content.

2.6. Preparation of biosensor electrodes

The working electrode with dimensions of 1cm×1.5cm was directly prepared by free-standing pure ECNF, Ni/ ECNF, NiO/ECNF, Co/ ECNF, Co_3O_4/ ECNF, Ni-Co/ ECNF, and $NiCo_2O_4$/ ECNF. No binder was employed and the electrode was implanted between two pieces of stainless steel while a part of it was exposed to electrolyte solution.

2.7. Morphological and structural characterizations

The microstructures and morphologies of the materials were studied on a field emission scanning electron microscope (FESEM, Mira 3-XMU, TESCAN Co.). The crystal structure was evaluated on an X-ray

diffraction (XRD) system (microanalyzerxmf-104) with Cu Kα radiation. Raman spectroscopy (Takram P50C0R10, Teksan) with a laser wavelength of 532 nm was used to characterize the degree of graphitization of electrodes. Thermogravimetric analysis (TGA) was conducted in the air over a temperature range of 50–800 °C with a heating rate of 10 °C min^{-1} using a STA 504. Nitrogen adsorption/desorption isotherms were obtained on a Belsorp mini II analyzer at 77 K. The specific surface areas were determined using the Brunauer–Emmett–Teller (BET) method. The electrical conductivity of samples was measured based on the two -point probe methods (2602A system source meter, keithley) at room temperature.

2.8. Electrochemical Measurements

All electrochemical measurements were performed in a beaker-type three-electrode system in 25cc of 0.1 M NaOH aqueous electrolyte at room temperature. A platinum plate and a saturated Ag/AgCl electrode were utilized as the counter electrode and reference electrode, respectively. The prepared electrodes were tested using a cyclic voltammetry (CV) method, chronoamperometric technique (I-t), and electrochemical impedance spectroscopy (EIS) technique on an Autolab PG STAT204N. The CV measurements were made at a potential window of 0.2-0.8 V at different scanning rates. EIS was performed at open circuit potential (OCP) with a frequency range from 10^{-2} - 10^{5} Hz and an alternating current (A.C.) voltage amplitude of 5mV in 0.1 M KCl solution containing 5mM $[Fe(C.N.)_6]^{3-/4-}$.

3. Results And Discussion

3.1. Structure characterizations of Co/ ECNF, Ni/ ECNF and Ni-Co / ECNF nanocomposites

With a combination of electrospinning and heat treatment techniques, metal N.P.s formed in-situ and grew on the surface of ECNFs. The mechanism of N.P.s formation at temperatures of about 250 ° C to 500 ° C, the metal salts ligand was thermally decomposed and pure metal remained. At temperatures of 650 to 1000 ° C, the ECNFs were formed from electrospun polymer nanofibers. As well, at high temperatures, metal N.P.s diffused from bulk of ECNFs to the surface due to the existence of metal concentration gradient between the bulk and ECNFs surface [28,29].

Fig. 1A-C showed FESEM images of Ni/ ECNF carbonized at T=1000°C and t=5hr, with different mass percentages of primary Ni precursor, i.e., 0.2 Ni/ ECNF, 0.35 Ni/ ECNF, and 0.5 Ni/ ECNF. Also, Fig. 1D-F displayed FESEM images of Co/ ECNF carbonized at T=800°C and t=5hr, with different mass percentages of primary Co precursor, i.e., 0.2 Co/ ECNF, 0.35 Co/ ECNF, and 0.5 Co/ ECNF. Furthermore, Fig. 1E and 1S displayed FESEM images of bimetallic Ni-Co/ ECNF carbonized at T=800°C and t=5hr. In all nanocomposites, metal N.P.s were uniformly dispersed on the surface of the ECNF with a narrow size distribution. When the percentage of metal salts precursor in the primary solution increased, the fiber diameters was smaller due to the lower carbon content in the nanocomposite. In all nanocomposites, ECNFs had a uniform bead-free morphology with diameters of about 200-400 nm and lengths of tens of

micrometers. Moreover, the loading percentage of N.P.s on ECNF surface increased with increasing the percentage of salt in the primary solution.

It was also found that the t_c parameter affected the metal N.P. sizes. For this purpose, 0.5 Ni/ ECNF and 0.5 Co/ ECNF nanocomposites were carbonized for 1, 3, and 5 hr. FESEM images and histograms of the size distribution of Ni and Co N.P.s on the surface of ECNF are shown in Figure S2 and S3, that the Ni particle sizes were 116.3 ± 4.3, 56.25 ± 3.6, 35.3 ± 3.1 nm respectively, for 0.5 Ni/ ECNF-1h, 0.5 Ni/ ECNF-3h and 0.5 Ni/ ECNF-5h. Also, for 0.5 Co/ ECNF-1h, 0.5 Co/ ECNF-3h and 0.5 Co/ ECNF-5h, the Co particle sizes were 52.8 ± 4.8, 48.05 ± 4.7, 46 ± 3.4 nm, respectively. It was observed that with increasing t_c, the size of Co and Ni N.P.s decreased. It was also seen that all the N.P.s had a narrow-size distribution at different carbonization times. Also, with increasing t_c from 1 to 5 h, due to increased nucleation and growth, the percentage of loading or the number of N.P.s on the surface of ECNFs increased.

Energy-dispersive X-ray spectroscopy (EDX) was applied to investigate compositions of Ni/ ECNF, Co/ ECNF, and Ni-Co/ ECNF nanocomposites. According to Figure 2A, the EDX spectrum of Ni/ ECNF confirmed the presence of C, Ni, N, and O elements. The presence of C, Co, N, and O elements in Co/ ECNF and presence of C, Ni, Co, N, and O elements in Ni-Co/ ECNF was also shown in Figure S2 A and B.

In addition, the weight percentages of C, Ni, O, and N elements in the 0.5 Ni/ ECNF-5h were 71.83, 16.42, 2.77, and 8.98 wt. %, respectively. The weight percentages of C, Co, O, and N elements were obtained in 0.5 Co/ECNF-5h nanocomposite of 66.35, 15.72, 4.48, and 13.45 wt. %, respectively. Also, weight percentages of C, Ni, Co, O, and N elements were obtained in $Ni_{70}Co_{30}$ / ECNF-5h of 65.61, 12.77, 5.81, 3.27 and 12.54 wt. %, respectively. The presence of nitrogen peak in the EDX spectrum was due to the presence of some nitrogen atoms on the surface of the final ECNFs, probably because PAN was used as the precursor for the synthesis of ECNFs [30].

Figures 2(B- C) and Fig. S4 (C-G) illustrated the map images of 0.5 Ni/ ECNFs, 0.5 Co/ ECNFs and $Ni_{70}Co_{30}$/ ECNF-5h nanocomposites. It was seen that the C, Ni, and Co elements were uniformly dispersed and present in the nanocomposites.

The XRD pattern of the monometallic Ni/ ECNF and Co/ ECNF nanocomposites and bimetallic Ni-Co/ ECNF nanocomposites are demonstrated in Figure 2D. We used XRD to further confirm the formation of the N.P.s and to investigate the crystalline structure of nanocomposites. The diffraction peaks with 2θ value of 26.52°, 23.0° and 26.14° in the Ni/ ECNF, Co/ ECNF and Ni-Co/ ECNF correspond to the (0 0 2) plane of the graphite structure in ECNF. For Ni/ ECNF, three sharp diffraction peaks at 2θ values of 44.5°, 51.8° and 76.4° were observed, corresponding to the (1 1 1), (2 0 0) and (2 2 0) crystalline planes of fcc Ni, respectively [31]. For Co/ ECNF, three sharp diffraction peaks at 2θ values of 44.4°, 51.4°, and 76.0°, corresponding to the (1 1 1), (2 0 0), and (2 2 0) crystalline planes of fcc Co, respectively [32]. Also, for bimetallic Ni-Co/ ECNF nanocomposite, three sharp diffraction peaks at 2θ values of 44.96°, 52.49°, and 76.83°, corresponding to the (1 1 1), (2 0 0), and (2 2 0) crystalline planes of fcc phase, respectively [33]. These results indicate that metal precursors have been completely converted into elemental metals.

Moreover, compared to Co/ ECNF, the diffraction peak of (0 02) plane in Ni/ ECNF nanocomposite has been shifted to 2θ of higher level indicating that the crystallinity percentage of carbon in Ni/ ECNF is higher than that of Co/ ECNF.

TGA was performed in air at a heating rate of 10 °C/min from 50-800 °C to study thermal stability and the percentage of metal N.P.s loading into the ECNF structure. According to Fig. 2E, a major weight loss was shown in the range of 350 to 450°C, which was related to the oxidation process of carbon nanofibers. The decomposition temperature of 0.5 Ni/ ECNF-5h nanocomposite was higher than that of 0.5 Co/ ECNF-5h nanocomposite. It was also seen that 0.5 Ni/ ECNF-5h and 0.5 Co/ ECNF-5h nanocomposites exhibited major weight loss at lower temperatures than that of pure ECNFs, possibly due to the higher thermal conductivity of ECNFs containing metal particles caused lower temperature degradation. However, it was also observed that the slope of the major weight loss in nanocomposites was lower than that of pure ECNFs. The percentages of Ni, Co and Ni/Co N.P.s loadings in the 0.5 Ni/ ECNF-5h, 0.5 Co/ ECNF-5h and $Ni_{70}Co_{30}$/ ECNF-5h nanocomposites were 41.4, 18.8 and 25.5 wt. %, respectively.

Raman spectroscopy was used to study the microstructure of CNFs containing metal more closely and to study the graphite structure and degree of graphitization of nanofibers. Carbon materials generally displayed two common peaks in Raman spectroscopy, known as D and G band peaks. The D band was associated with disorder due to structural defects in carbon, and the G band was related to the stretching vibrations of the ordered sp^2 bonding carbon atoms in the graphitic layers, as seen in Figure 3 A-C [34,35]. Figures S 5 demonstrated the Raman spectra of Ni/ ECNF and Co/ ECNF and the effect of metal precursors percentage and t_c on the intensities of D and G peaks. Also, Figures S 5 showed Raman spectra of bimetallic Ni-Co nanocomposites with different percentages of Ni and Co precursors.

In Table 1, the Raman spectroscopy results of Ni/ ECNF and Co/ ECNF nanocomposites were presented. $I_{.D.}$ (intensity of D band peak), $I_{.G.}$ (intensity of G band peak), I_D/I_G ratio (R ratio), the degree of graphitization, and the average crystallite size (L_a) were calculated. The degree of graphitization was estimated by the intensity $\text{ratio: } = \frac{I_G}{I_D+I_G} \times 100$ [36]. The average crystallite size was estimated through the following equation: in which λ is the wavelength of laser [37]

$$L_a(\text{average crystallite size}) = 2.4 \times 10^{-10} \times \lambda_{\text{laser}}^4 \times \frac{I_G}{I_D}.$$

According to Tables 1, with increasing metal salt precursor percentages from 0.2 to 0.5 g in both Ni/ ECNF and Co/ ECNF nanocomposites, the R ratio value decreased, and the degree of graphitization and the average crystallite size increased. This indicated that the structural order and crystallinity percentage of ECNFs increased [38]. It was also observed that with increasing t_c, the crystallinity percentage of nanocomposites increased. The higher the degree of graphitization and the crystallinity percentage of the ECNFs, the greater the electrical conductivity and the better the substrate for biosensor application [39]. In

addition, it is important to note that the R ratio values for Ni-containing composites were lower than those of Co-containing composites, indicating that Ni metal had a higher ability to graphitize ECNFs.

Table 1 : D and G peaks intensity, R ratios, degree of graphitization, and estimated La values of Ni/ ECNF and Co/ ECNF nanocomposites with different t_c and metal salt precursor contents.

Sample name	$I_D(\%)$ $1300-1400\ cm^{-1}$	$I_G(\%)$ $1580-1600\ cm^{-1}$	$R=\frac{I_D}{I_G}$	Degree of graphitization	La(average crystallite sise)
0.5 Ni/ ECNF-1h	58.239	71.965	0.809	55.27	5.412
0.5 Ni/ ECNF-3h	40.792	90.066	0.453	68.827	9.67
0.5 Ni/ ECNF-5h	43.121	103.839	0.415	70.658	10.547
0.35 Ni/ ECNF-5h	57.852	74.715	0.77	56.36	5.656
0.2 Ni/ ECNF-5h	55.256	65.116	0.85	54.095	5.161
0.5 Co/ ECNF-1h	29.274	30.383	0.96	50.929	4.545
0.5 Co/ ECNF-3h	32.506	34.519	0.94	51.501	4.651
0.5 Co/ ECNF-5h	26.846	34.519	0.77	56.321	5.647
0.35 Co/ ECNF-5h	36.666	41.7	0.88	53.211	4.981
0.2 Co/ ECNF-5h	25.826	26.905	0.96	51.023	4.562

Raman data of bimetallic nanocomposites are presented in Table S1. It is observed that with increasing the amount of Ni precursor in the initial solution, the value of R ratio decreases, and the degree of graphitization increases, as shown for $Ni_{70}Co_{30}$/ ECNF-5h sample, with the maximum degree of carbon graphitization. Afterward, the degree of graphitization decreases with a further rise of Ni precursor in the solution.

At the carbonization stage, the metallic precursor was converted to metallic N.P.s, which acted as catalysts to crystallize amorphous carbon and create hexagonal graphite structures [40]. Graphitization around the metal N.P.s occurs during the heat treatment involved the dissolution of amorphous carbon into catalyst particles, followed by the precipitation of graphitic carbon[19,41]. The presence of graphite not only increased the electrical conductivity of the ECNFs substrate, which increased the sensitivity of the biosensor but also prevented the N.P.s from being separated from ECNFs matrix [42].

The testing voltage ranged from 0 V to 1V for conductivity assessment on Keithley instrument. The measurement was done for 5 times under the same conditions. The average I -V curve is shown in Fig. S6. The values of conductance, thickness and electrical conductivity of nanocomposites are given in Table 2 and Table S2. According to Table 2, it was observed that with increasing the percentage of the metal precursors in the composition, the electrical conductivity of the nanocomposite increased. In fact, as the metal catalyst content in the nanocomposite system increased, the degree of graphitization of ECNFs increased, and the graphite structure became more arranged [43]. Also, according to Table 2, increasing the t_c had a significant effect on the electrical conductivity of the samples. Time parameter was another influential parameter on the degree of carbon graphitization in a way that the longer the t_c, the more structural order in carbon, and the higher the degree of graphitization and electrical conductivity

of ECNFs. At the same t_c and at the same percentage of metal salts precursor in the two Ni/ ECNF and Co/ ECNF nanocomposites, it was observed that the electrical conductivity of the Ni-based nanocomposite was higher than that of Co-based nanocomposite due to the higher Ni catalyst graphitization ability in the substrate of ECNFs. Furthermore, according to Table S2, with increasing the percentage of Ni in the bimetallic system, the electrical conductivity of the electrode increases, so that for $Ni_{70}Co_{30}$/ ECNF-5h, with the combination of Ni $(acac)_2$ / CoAc: 0.35 / 0.15 g, the highest electrical conductivity was obtained. Therefore, the results of electrical conductivity were in agreement with the results of Raman spectroscopy.

Table 2 : Electrical Conductivities of Ni/ ECNF and Co/ ECNF Nanocomposites with different t_c and metal salt precursor contents.

Sample name	Conductance=1/R (S)	Thickness of samples (μm)	Electrical conductivity (S/cm)
0.5 Ni/ ECNF-1h	0.016	75	2.13
0.5 Ni/ ECNF-3h	0.064	60	10.66
0.5 Ni/ ECNF-5h	0.076	64	11.87
0.35 Ni/ ECNF-5h	0.052	72	7.22
0.2 Ni/ ECNF-5h	0.037	61	6.06
0.5 Co/ ECNF-1h	0.0084	62	1.35
0.5 Co/ ECNF-3h	0.0094	65	1.45
0.5 Co/ ECNF-5h	0.046	68	6.76
0.35 Co/ ECNF-5h	0.036	66	5.45
0.2 Co/ ECNF-5h	0.01	63	1.59

The nitrogen adsorption/desorption isotherms are shown in Figure S7, and the BET specific surface areas of Ni/ ECNF and Co/ ECNF nanocomposites, and pure ECNFs were summarized in Table 3. It was observed that the specific surface area of the metal-containing nanofibers were higher than those of the pure nanofibers, which was due to the exhaled gases from the thermal decomposition of the metal precursor ligand. Moreover, through increasing the metal salt precursor content in nanocomposites, the specific surface area increased [44]. The higher surface area facilitated ion penetration between the electrode and the electrolyte and facilitated electron transfer rate, which had a favorable effect on the biosensor sensitivity.

Table 3 : Specific surface areas of pure ECNF and nanocomposites of Ni/ ECNF and Co/ ECNF prepared with different metal salt precursor contents.

Sample name	surface area ($m^2.g^{-1}$)
pure ECNF	30.7
0.2 Ni/ ECNF-5h	65.8
0.35 Ni/ ECNF-5h	153.4
0.5 Ni/ ECNF-5h	209.7
0.2 Co/ ECNF-5h	46.5
0.35 Co/ ECNF-5h	131.9
0.5 Co/ ECNF-5h	154.2

3.2. Electrochemical measurements and Electrocatalytic oxidation of glucose

All electrodes were prepared free standing without the need for a binder and GCE in order to bring the electrode to the actual glucometer strips and to be employed in practical applications.

In order to investigate the electrochemical properties of the electrodes, CV analysis was performed with the potential range from 0.2 to 0.8 V in 0.1 M NaOH aqueous solution in absence (black line) and presence (red line) of 4 mM glucose at a scan rate of 50 mVs^{-1}. According to Fig. 4(B-D) (black line), a pair of redox peaks was observed in the potential range of 0.25 - 0.65V, corresponding to the reversible redox reactions of Ni(II)/Ni(III) and Co(II)/Co(III) redox couple in the alkaline media [24,45]. In addition, in comparison with Co/ ECNF electrode, the Ni/ ECNF electrode showed lower anodic peak potentials and higher anodic peak current. It reflects easier electron transfer kinetics and facilitated Ni(II)/Ni(III) redox processes of Ni/ ECNF than Co/ ECNF due to the higher electrical conductivity and higher specific surface area of Ni/ ECNF nanocomposite. Also, as shown in Fig. 4 A (black line), it was observed that pure ECNFs exhibited no redox peak during the scan potential. Therefore, Ni and Co acted as excellent electrocatalysts in nanocomposites.

After the addition of 4mM glucose into the 0.1 M NaOH solution, it was observed that for the pure ECNF, no oxidation and reduction peak was perceived and CV curves show the same behavior in the absence and presence of glucose. This indicated that pure ECNF had no electrocatalytic activity toward the glucose oxidation reaction. For 0.5 Ni/ ECNF-5h, 0.5 Co/ ECNF-5h and $Ni_{70}Co_{30}$/ ECNF-5h nanocomposites, a pair of oxidation and reduction peak was observed in the potential range of 0.65 and 0.25 V, respectively, corresponding to the redox pair of Ni (II)/Ni (III) and Co (II)/Co (III) formed in the alkaline media. After the addition of 4mM glucose into the 0.1 M NaOH solution, it was observed that the anodic peak current of 0.5 Ni/ ECNF-5h, 0.5 Co/ ECNF-5h and $Ni_{70}Co_{30}$/ ECNF-5h electrodes increased at ca. 0.55, 0.6 and 0.65V respectively, indicating that the Ni and Co N.P.s on the surface of the ECNFs were capable of catalyzing the glucose oxidation reaction. It was also observed that the anodic peak current of Co/ ECNF nanocomposites was lower than that of Ni/ ECNF nanocomposites. This result suggested that Ni/ ECNF was much more sensitive than Co/ ECNF to changes in glucose concentration.

Furthermore, to investigate the effect of t_c on electrochemical properties, the CV analysis was conducted on Ni/ ECNF electrodes synthesized with different t_c of 1, 3, and 5 h. As shown in Figure 4 E, with increasing t_c from 1 to 5 h, the anodic peak potential decreased and anodic peak current increased due to the increased electrical conductivity with increasing t_c. This result also held true for Co/ ECNF nanocomposites (the data are not shown here).

Figure 4F illustrated the effect of glucose concentration on the anodic peak current of Ni/ ECNF nanocomposites in the CV. It was observed that the anodic peak current increased with an increase in glucose concentration, indicating high electrode sensitivity in glucose oxidation reaction. EIS technique was also performed to better understand the electrochemical properties of 0.5 Ni/ ECNF-5h, 0.5 Co/ ECNF-5h and $Ni_{70}Co_{30}$/ ECNF-5h nanocomposites, and the Nyquist plots are displayed in Fig. 5A. The electron transfer resistance (R_{ct}), known as the electron transfer kinetics at the electrode interface, was measured using EIS. The R_{ct} value of 0.5 Ni/ ECNF-5h electrode was smaller than that of the 0.5 Co/ ECNF-5h electrode, indicating easier electron transfer kinetics and higher electron transfer rate during redox processes in the Ni/ ECNF composite. Also, R_{ct} value of $Ni_{70}Co_{30}$/ ECNF-5h electrode was smaller than that of the 0.5 Co/ ECNF-5h electrode. Therefore, the impedance test results confirmed the results of CV study. The effect of scanning rate on the oxidation response of 2.0 mM glucose in aqueous solution of 0.1M NaOH was investigated via CV analysis. According to Fig. 5B, the anodic peak current increased with increasing scan rate in the range of 10 to 200 mVs^{-1}. Also, the anodic peak currents were proportional to the square root of the scan rate (Fig. 5C). This indicates that the glucose oxidation reaction at the electrode interface was a diffusion controlled process well corresponded to the EIS results.

3. 3. Amperometric sensing of glucose at the electrodes

The convenient production method and low-cost of free-standing electrodes, without the need for a glassy carbon electrode and binders and, together with high electrocatalytic performance, converted N.P.s/ ECNFs nanocomposites into electrodes with a suitable electrochemical sensing for amperometric detection of glucose. Initially, the effect of applied potential on the current response was investigated to achieve the highest current responses. As shown in Figure 5D, for 0.5 Ni/ ECNF-5h nanocomposite with potential variations ranging from 0.25 to 0.65V, the maximum current response was obtained at a potential of 0.5V. Whereas, for 0.5 Co/ ECNF-5h and $Ni_{70}Co_{30}$/ ECNF-5h nanocomposites, this maximum current occurred at a potential of 0.6V and 0.55V, respectively (Fig. 5 D). Therefore, the values of 0.5, 0.6 and 0.55V for Ni/ ECNF, Co/ ECNF and Ni-Co/ ECNF nanocomposites were selected as optimum applied potentials for amperometric experiments of glucose, respectively. Hence, the chronoamprometric analysis was conducted on Ni/ ECNF, Co/ ECNF and Ni-Co/ ECNF free-standing electrodes with different percentages of the metallic salt precursor (in the same t_c of 5 h).

Figure 6A displayed the chronoamperometric responses of Ni/ ECNF nanocomposites with different percentages of metal salt precursor, namely 0.2 Ni/ ECNF-5h, 0.35 Ni/ ECNF-5h, and 0.5 Ni/ ECNF-5h after sequential addition of glucose solutions with constant concentrations of 2 mM in the each time of

injection. It was observed that as the percentage of metal salt precursor increased, the amperometric current response increased. The calibration plot of the samples in Figure 6B demonstrated that as the catalyst percentage in the nanocomposite increased, the slope of the calibration curve, was increased. It is obtained due to the increased electrical conductivity and specific surface area resulting in the biosensor sensitivity to glucose,. Therefore, the highest sensitivity, i.e., 610.6 μA mM^{-1} cm^{-2}, was found for 0.5 Ni/ ECNF-5h. Also, all the electrodes in the range of 2 - 10 mM showed a linear response to glucose concentration changes. Figure 6C also illustrated the chronoamperometric responses of Co/ ECNF nanocomposites with different percentages of cobalt metal salts. Again, by increasing the Co precursor value to 0.5g, the current response and sensitivity of the biosensor increased. The calibration plot of these samples in Figure 6D demonstrated that the highest sensitivity value for the sample was 0.5 Co/ ECNF-5h with a value of 236.85 μA mM^{-1} cm^{-2}. The linear range of 2 - 10 mM was also obtained for all samples. It is also worth noting that at the same percentage of salt precursor, the current response and the sensitivity of Ni/ ECNF nanocomposite was much higher than that of the Co/ ECNF nanocomposite. It indicates that Ni catalyst had a higher ability in comparison with Co to graphitize carbon. The results of the chronoamprometric test confirmed the results of Raman test and electrical conductivity. In addition, Ni catalysts probably had higher electrocatalytic properties toward the glucose oxidation reaction.

The chronoamprometric diagram of bimetallic Ni and Co nanocomposites is also illustrated in Figure 6E. It can be observed that with increasing the amount of Ni precursor in bimetallic Ni-Co nanocomposites. The sensitivity of the resulting biosensor is increased so that it reaches its maximum value at $Ni_{70}Co_{30}$/ ECNF-5h electrode (498.53 μA mM^{-1} cm^{-2}). As well, it is important to mention that the sensitivity of $Ni_{70}Co_{30}$/ ECNF-5h bimetal biosensor is nearly twice that of 0.5 Co/ ECNF-5h monometal biosensor. Moreover, the chronoamprometric analysis was also conducted on samples of NiO/ ECNF, Co_3O_4/ ECNF and $NiCo_2O_4$/ ECNF. According to Figure 7A, the sample of NiO/ ECNF exhibited lower current responses and sensitivity than that of 0.5 Ni/ ECNF-5h. In fact, it can be mentioned that Ni/ ECNF nanocomposites had higher electrocatalytic properties than NiO/ ECNF toward glucose oxidation reaction. Furthermore, the result of chronoamperometric test of 0.5 Co/ ECNF-5h and Co_3O_4/ ECNF samples in Figure 7C revealed that the Co_3O_4/ ECNF sample had higher electrocatalytic properties toward glucose and was more sensitive than 0.5 Co/ ECNF-5h sample.

Moreover, in order to compare the sensor performance of $Ni_{70}Co_{30}$/ ECNF-5h with $NiCo_2O_4$/ ECNF, the chronoamprometric test of the samples is demonstrated in Figure 7E. According to Figure 7F, the slope of the calibration curve and the sensitivity of $NiCo_2O_4$/ ECNF were assessed higher than that of Ni70Co30 / ECNF-5h. The results of the sensitivity, linear range, and detection limit of the electrodes were summarized in Table 4.

Table 4 : Values of Sensitivity, linear range and detection limit of manufactured electrodes.

Sample name	Sensitivity ($\mu A.\ mM^{-1}.\ cm^{-2}$)	Linear range (mM)	LOD (mM)
0.2 Ni/ ECNF-5h	344.37	2-10	0.89
0.35 Ni/ ECNF-5h	516.42	2-10	0.78
0.5 Ni/ ECNF-5h	610.6	2-10	0.73
NiO/ ECNF	557.68	2-10	0.85
0.2 Co/ ECNF-5h	66.28	2-10	0.99
0.35 Co/ ECNF-5h	131.77	2-10	0.76
0.5 Co/ ECNF-5h	236.85	2-10	0.61
Co_3O_4/ ECNF	475.72	2-10	0.82
$Ni_{90}Co_{10}$/ ECNF-5h	414.45	2-10	0.98
$Ni_{70}Co_{30}$/ ECNF-5h	498.53	2-10	0.91
$Ni_{50}Co_{50}$/ ECNF5h	405.48	2-10	0.96
$Ni_{30}Co_{70}$/ ECNF-5h	364.68	2-10	0.97
$Ni_{10}Co_{90}$/ ECNF-5h	358.01	2-10	0.99
$NiCo_2O_4$/ ECNF	536.5	2-10	0.93

The performance of the biosensors developed in this study was compared with similar nonenzymatic glucose biosensors. As shown in Table 5, it is clearly evident that, in the present investigation, the carbon-based electrodes included a high sensitivity and a wide linear range. The good performance of the electrodes can be attributed to the excellent electrocatalytic properties of Ni and Co N.P.s besides the enhanced electrical conductivity of ECNFs due to the addition of these catalysts.

Table 5 : Comparison of the performance of our proposed biosensors with other nonenzymatic glucose biosensors based on carbon nanomaterials and metal-based nanoparticles.

Electrode	Sensitivity ($\mu A.mM^{-1}.cm^{-2}$)	Linear range (mM)	LOD (mM)	References
NiCFP[a] electrode	420.4	0.002-2.5	10^{-3}	[24]
Ni powder sol gel ceramic graphite composite	0.04 $\mu A.mM^{-1}$	5×10^{-4}-5	-	[47]
Pd–Ni/CNF	-	0.00003-0.8	7×10^{-6}	[9]
$Ni(O.H.)_2$/CNFs/GCE	1038.6	0.001–1.2	0.76	[48]
Electrospun Co_3O_4 nanofibers	36.25	Up to 2.04	97×10^{-5}	[26]
Ni/ITO[b]	189.5	0.001–0.35	5×10^{-4}	[49]
NiO/OMC[c]/GCE	834.8	0.002–1	65×10^{-5}	[25]
Co_3O_4/flexible carbon cloth	64.71	5×10^{-4}-1	12×10^{-6}	[50]
CoO nanorods	571.8	Up to 3.5	0.000058	[51]
0.5 Ni/ ECNF-5h	610.6	2-10	0.78	This work
NiO/ ECNF	557.68	2-10	0.85	This work
0.5 Co/ ECNF-5h	236.85	2-10	0.61	This work
Co_3O_4/ ECNF	475.72	2-10	0.82	This work
$Ni_{70}Co_{30}$/ ECNF-5h	498.53	2-10	0.91	This work
$NiCo_2O_4$/ ECNF	536.5	2-10	0.93	This work

[a] Ni nanoparticle-loaded carbon nanofibers paste.

[b] indium tin oxide.

[c] ordered mesoporous carbon.

3. 4. Selectivity of electrodes

In the real human blood sample, there are some electrochemically active and other oxidizable interferences such as A.A., U.A., and DA which may interfere. Therefore, selectivity is one of the key factors in evaluating the performance of nonenzymatic glucose biosensors. Typically, the normal physiological level of glucose in the blood is about 3 - 8 mM, while the concentration of the aforementioned interfering agents is about 0.1 mM [52]. In addition, the chronoamperometric test of electrodes was performed in 0.1 M NaOH solution by successive addition of interfering species and glucose. As shown in Figure 8, none of the electrodes exhibited a significant current response to the interfering agents. Therefore, all electrodes had excellent selectivity for the detection of glucose in the presence of potential disturbing agents. Good selectivity may be due to the use of lower applied potentials, which could be resulted from higher electrical conductivity and easier electron transfer of ECNF-based nanocomposites.

3. 5. Stability, reproducibility and real samples measurement of the biosensor

The electrodes were stored at room temperature for 5 weeks and amperometric test was carried out to investigate the long-term stability. There was no significant change in the biosensor current response. The

high stability of the biosensor was due to the presence of ECNFs matrix and encapsulation of the N.P.s, which prevented the N.P.s from being separated from the ECNFs matrix. Moreover, reproducibility was evaluated for 3 different electrodes in 4 mM glucose, in which the relative standard deviation (RSD) was 3.24%. In addition, the developed electrode was tested to determine the glucose concentration of human serum samples. Thus, 100 µl of the serum sample was added to 25 ml of 0.1 M NaOH solution and the current response was measured. The glucose concentration measured by the electrode was 4.6 mM, which was close to the data obtained by a commercial glucometer (4.47 mM).

Conclusions

Nanocomposites of ECNF decorated with different Ni/Co complexes were in-situ prepared using electrospinning of polymer and metal precursors. Then the thermal treatment process was performed to decrease metals and carbonize PAN nanofibers. Ultimately free-standing electrodes were conveniently and successfully made with no need for binders. FESEM and XRD techniques were applied to study morphology and crystalline structure of the synthesized nanocomposites. The metal-based N.P.s were uniformly dispersed on the surface of ECNFs. Raman spectroscopy and electrical conductivity techniques were employed to investigate the structure of nanocomposites, graphitization degree, and electrodes' conductivity. The prepared electrodes were also tested using a CV method and chronoamperometric technique. Free-standing electrodes of monometal, bimetal, and oxide compounds of Ni and Co elements grown on ECNFs exhibited a pair of redox peaks in the alkaline electrolyte solution. 0.5 Ni/ ECNF-5h, 0.5 Co/ ECNF-5h, NiO/ ECNF, Co_3O_4/ ECNF, $Ni_{70}Co_{30}$/ ECNF-5h and $NiCo_2O_4$/ ECNF non-enzymatic glucose biosensors exhibited excellent performance towards the glucose oxidation reaction. The use of electrodes in real human blood samples was also successfully investigated. Low detection limit, wide linear range, high sensitivity, good selectivity, and favorable reproducibility of the prepared glucose biosensors, convenient manufacturing method, and low cost, all together converted such electrodes to a fine and promising candidate for producing nonenzymatic biosensors for glucose diagnosis.

Declarations

Funding: This study was not funded by any grant, institute or government.

Conflict of Interest: The authors declare that they have no conflict of interest.

-**Ethical Approval** : Not applicable

Consent to Participate : It is given as follows

Consent to Publish : It is given as follows

Authors Contributions : It is given as follows : Ali Mohammadpour-Haratbar "AMH", Saeedeh Mazinani "SM", Farhad Sharif "FS", Ali Mohammad Bazargan "AMB"

Funding : Not applicable

Competing Interests: Not applicable

Availability of data and materials: Not applicable

The work submitted to " Applied Biochemistry & Biotechnology " is a quite novel work in the field of non-enzymatic biosensors for glucose analysis. To the best of our knowledge, the work is quite new regarding low-cost, free-stand glucose biosensor manufacturing. The proposed sensors include a wide linear range, high sensitivity and proper selectivity towards the oxidation of glucose.

Moreover, hereby, I certify that this is an original work of the group and it has been written by the stated authors (Ali Mohammadpour-Haratbar “AMH”, Saeedeh Mazinani ″SM”, Farhad Sharif ″FS”, Ali Mohammad Bazargan “AMB”) who are all aware of its content and approve its submission. This work has not submitted, not accepted, and not under consideration for publication in any other journal. The paper and information won't be published in any other journal in any language if accepted in " Applied Biochemistry & Biotechnology ". Moreover, no conflict exists and all authors have agreed upon this submission and they are aware of the content. Considering the recent works published in your journal and the scope of your journal, we selected " Applied Biochemistry & Biotechnology " for this submission. Therefore, I would really appreciate if you consider this work for review and further steps in your journal. Your great concern is highly appreciated in advanced.

Best Regards,

Saeedeh Mazinani (PhD)

New technologies research center (NTRC); Amirkabir University of Technology, Tehran, IRAN. E-mail: s.maziani@aut.ac.ir

Phone No.: +98-21-64545710

References

[1] N.J. Ronkainen, H.B. Halsall, W.R. Heineman, Electrochemical biosensors, Chem. Soc. Rev. 39 (2010) 1747–1763.

[2] C. Chen, Q. Xie, D. Yang, H. Xiao, Y. Fu, Y. Tan, S. Yao, Recent advances in electrochemical glucose biosensors: a review, Rsc Adv. 3 (2013) 4473–4491.

[3] R. Wilson, A.P.F. Turner, Glucose oxidase: an ideal enzyme, Biosens. Bioelectron. 7 (1992) 165–185.

[4] Y. Zhang, L. Luo, Z. Zhang, Y. Ding, S. Liu, D. Deng, H. Zhao, Y. Chen, Synthesis of MnCo 2 O 4 nanofibers by electrospinning and calcination: application for a highly sensitive non-enzymatic glucose sensor, J. Mater. Chem. B. 2 (2014) 529–535.

[5] Y.-W. Hsu, T.-K. Hsu, C.-L. Sun, Y.-T. Nien, N.-W. Pu, M.-D. Ger, Synthesis of CuO/graphene nanocomposites for nonenzymatic electrochemical glucose biosensor applications, Electrochim. Acta. 82 (2012) 152–157.

[6] J. Zhang, J. Ma, S. Zhang, W. Wang, Z. Chen, A highly sensitive nonenzymatic glucose sensor based on CuO nanoparticles decorated carbon spheres, Sensors Actuators, B Chem. 211 (2015) 385–391. https://doi.org/10.1016/j.snb.2015.01.100.

[7] N. Lu, C. Shao, X. Li, F. Miao, K. Wang, Y. Liu, CuO nanoparticles/nitrogen-doped carbon nanofibers modified glassy carbon electrodes for non-enzymatic glucose sensors with improved sensitivity, Ceram. Int. 42 (2016) 11285–11293. https://doi.org/10.1016/j.ceramint.2016.04.046.

[8] Y.L. Hsin, K.C. Hwang, C.-T. Yeh, Poly (vinylpyrrolidone)-modified graphite carbon nanofibers as promising supports for PtRu catalysts in direct methanol fuel cells, J. Am. Chem. Soc. 129 (2007) 9999–10010.

[9] Q. Guo, D. Liu, X. Zhang, L. Li, H. Hou, O. Niwa, T. You, Pd–Ni alloy nanoparticle/carbon nanofiber composites: preparation, structure, and superior electrocatalytic properties for sugar analysis, Anal. Chem. 86 (2014) 5898–5905.

[10] J.-G. Wang, Y. Yang, Z.-H. Huang, F. Kang, Coaxial carbon nanofibers/MnO2 nanocomposites as freestanding electrodes for high-performance electrochemical capacitors, Electrochim. Acta. 56 (2011) 9240–9247.

[11] E.S. Steigerwalt, G.A. Deluga, D.E. Cliffel, C.M. Lukehart, A Pt- Ru/graphitic carbon nanofiber nanocomposite exhibiting high relative performance as a direct-methanol fuel cell anode catalyst, J. Phys. Chem. B. 105 (2001) 8097–8101.

[12] J. Huang, D. Wang, H. Hou, T. You, Electrospun palladium nanoparticle-loaded carbon nanofibers and their electrocatalytic activities towards hydrogen peroxide and NADH, Adv. Funct. Mater. 18 (2008) 441–448.

[13] J. Zhang, Z. Zhu, C. Chen, Z. Chen, M. Cai, B. Qu, T. Wang, M. Zhang, ZnO-carbon nanofibers for stable, high response, and selective H2S sensors, Nanotechnology. 29 (2018) 275501.

[14] K. Cui, Y. Song, Q. Guo, F. Xu, Y. Zhang, Y. Shi, L. Wang, H. Hou, Z. Li, Architecture of electrospun carbon nanofibers–hydroxyapatite composite and its application act as a platform in biosensing, Sensors Actuators B Chem. 160 (2011) 435–440.

[15] S.K. Nataraj, K.S. Yang, T.M. Aminabhavi, Polyacrylonitrile-based nanofibers—A state-of-the-art review, Prog. Polym. Sci. 37 (2012) 487–513.

[16] S.-J. Park, S.-H. Im, Electrochemical behaviors of PAN/Ag-based carbon nanofibers by electrospinning, Bull. Korean Chem. Soc. 29 (2008) 777–781.

[17] G. Hu, Z. Zhou, Y. Guo, H. Hou, S. Shao, Electrospun rhodium nanoparticle-loaded carbon nanofibers for highly selective amperometric sensing of hydrazine, Electrochem. Commun. 12 (2010) 422–426.

[18] W. Weisweiler, N. Subramanian, B. Terwiesch, Catalytic influence of metal melts on the graphitization of monolithic glasslike carbon, Carbon N. Y. 9 (1971) 755–761.

[19] H. Zhou, Q. Yu, Q. Peng, H. Wang, J. Chen, Y. Kuang, Catalytic graphitization of carbon fibers with electrodeposited Ni–B alloy coating, Mater. Chem. Phys. 110 (2008) 434–439.

[20] S.K. Vashist, D. Zheng, K. Al-Rubeaan, J.H.T. Luong, F.-S. Sheu, Technology behind commercial devices for blood glucose monitoring in diabetes management: A review, Anal. Chim. Acta. 703 (2011) 124–136.

[21] A.D. Association, others, Diagnosis and classification of diabetes mellitus, Diabetes Care. 37 (2014) S81–S90.

[22] A. Sedighi, M. Montazer, S. Mazinani, Synthesis of wearable and flexible NiP0. 1-SnOx/PANI/CuO/cotton towards a non-enzymatic glucose sensor, Biosens. Bioelectron. 135 (2019) 192–199.

[23] Y. Li, Y.-Y. Song, C. Yang, X.-H. Xia, Hydrogen bubble dynamic template synthesis of porous gold for nonenzymatic electrochemical detection of glucose, Electrochem. Commun. 9 (2007) 981–988.

[24] Y. Liu, H. Teng, H. Hou, T. You, Nonenzymatic glucose sensor based on renewable electrospun Ni nanoparticle-loaded carbon nanofiber paste electrode, Biosens. Bioelectron. 24 (2009) 3329–3334. https://doi.org/10.1016/j.bios.2009.04.032.

[25] L. Luo, F. Li, L. Zhu, Y. Ding, Z. Zhang, D. Deng, B. Lu, Nonenzymatic glucose sensor based on nickel (II) oxide/ordered mesoporous carbon modified glassy carbon electrode, Colloids Surfaces B Biointerfaces. 102 (2013) 307–311.

[26] Y. Ding, Y. Wang, L. Su, M. Bellagamba, H. Zhang, Y. Lei, Electrospun Co3O4 nanofibers for sensitive and selective glucose detection, Biosens. Bioelectron. 26 (2010) 542–548.

[27] L. Liu, Z. Wang, J. Yang, G. Liu, J. Li, L. Guo, S. Chen, Q. Guo, NiCo2O4 nanoneedle-decorated electrospun carbon nanofiber nanohybrids for sensitive non-enzymatic glucose sensors, Sensors Actuators B Chem. 258 (2018) 920–928.

[28] R.K. Sharma, R. Ghose, Synthesis of porous nanocrystalline NiO with hexagonal sheet-like morphology by homogeneous precipitation method, Superlattices Microstruct. 80 (2015) 169–180.

[29] L. Niinisto, M. Utriainen, M. Kroger-Laukkanen, L.S. Johansson, Studies of metallic thin film growth in an atomic layer epitaxy reactor using M (acac) sub 2(M= Ni, Cu, Pt) precursors, Appl. Surf. Sci. 157 (2000) 151–158.

[30] M. Wu, Q. Wang, K. Li, Y. Wu, H. Liu, Optimization of stabilization conditions for electrospun polyacrylonitrile nanofibers, Polym. Degrad. Stab. 97 (2012) 1511–1519.

[31] L. Li, T. Zhou, G. Sun, Z. Li, W. Yang, J. Jia, G. Yang, Ultrasensitive electrospun nickel-doped carbon nanofibers electrode for sensing paracetamol and glucose, Electrochim. Acta. 152 (2015) 31–37. https://doi.org/10.1016/j.electacta.2014.11.048.

[32] C. An, Y. Wang, Y. Xu, Y. Wang, Y. Huang, L. Jiao, H. Yuan, In situ preparation of 1D Co@ C composite nanorods as negative materials for alkaline secondary batteries, ACS Appl. Mater. Interfaces. 6 (2014) 3863–3869.

[33] D.-E. Zhang, X.-M. Ni, X.-J. Zhang, H.-G. Zheng, Synthesis and characterization of Ni–Co needle-like alloys in water-in-oil microemulsion, J. Magn. Magn. Mater. 302 (2006) 290–293.

[34] C. Kim, S.-H. Park, J.-I. Cho, D.-Y. Lee, T.-J. Park, W.-J. Lee, K.-S. Yang, Raman spectroscopic evaluation of polyacrylonitrile-based carbon nanofibers prepared by electrospinning, J. Raman Spectrosc. 35 (2004) 928–933.

[35] Y. Wang, S. Serrano, J.J. Santiago-Avilés, Raman characterization of carbon nanofibers prepared using electrospinning, Synth. Met. 138 (2003) 423–427.

[36] T.D. Nguyen Van, S. Sufian, N. Mansor, N. Yahya, Characterization of carbon nanofibers treated with thermal nitrogen as a catalyst support using point-of-zero charge analysis, J. Nanomater. 2014 (2014).

[37] L.G. Cançado, K. Takai, T. Enoki, M. Endo, Y.A. Kim, H. Mizusaki, A. Jorio, L.N. Coelho, R. Magalhaes-Paniago, M.A. Pimenta, General equation for the determination of the crystallite size L a of nanographite by Raman spectroscopy, Appl. Phys. Lett. 88 (2006) 163106.

[38] T. Kim, J. Lee, K.-H. Lee, Full graphitization of amorphous carbon by microwave heating, RSC Adv. 6 (2016) 24667–24674.

[39] D. Li, G. Li, P. Lv, N. Ullah, C. Wang, Q. Wang, X. Zhang, Q. Wei, Preparation of a graphene-loaded carbon nanofiber composite with enhanced graphitization and conductivity for biosensing applications, RSC Adv. 5 (2015) 30602–30609.

[40] A. \=Oya, S. \=Otani, Catalytic graphitization of carbons by various metals, Carbon N. Y. 17 (1979) 131–137.

[41] A. \=Oya, H. Marsh, Phenomena of catalytic graphitization, J. Mater. Sci. 17 (1982) 309–322.

[42] N.A.M. Barakat, B. Kim, S.J. Park, Y. Jo, M.-H. Jung, H.Y. Kim, Cobalt nanofibers encapsulated in a graphite shell by an electrospinning process, J. Mater. Chem. 19 (2009) 7371–7378.

[43] Y. Wang, S. Serrano, J.J. Santiago-Aviles, Conductivity measurement of electrospun PAN-based carbon nanofiber, J. Mater. Sci. Lett. 21 (2002) 1055–1057.

[44] W.-H. Ryu, J. Shin, J.-W. Jung, I.-D. Kim, Cobalt (II) monoxide nanoparticles embedded in porous carbon nanofibers as a highly reversible conversion reaction anode for Li-ion batteries, J. Mater. Chem. A. 1 (2013) 3239–3243.

[45] Y. Li, M. Xie, X. Zhang, Q. Liu, D. Lin, C. Xu, F. Xie, X. Sun, Co-MOF nanosheet array: A high-performance electrochemical sensor for non-enzymatic glucose detection, Sensors Actuators B Chem. 278 (2019) 126–132.

[46] Y. Liu, H. Teng, H. Hou, T. You, Nonenzymatic glucose sensor based on renewable electrospun Ni nanoparticle-loaded carbon nanofiber paste electrode, Biosens. Bioelectron. 24 (2009) 3329–3334.

[47] A. Salimi, M. Roushani, Non-enzymatic glucose detection free of ascorbic acid interference using nickel powder and nafion sol–gel dispersed renewable carbon ceramic electrode, Electrochem. Commun. 7 (2005) 879–887.

[48] L. Zhang, S. Yuan, X. Lu, Amperometric nonenzymatic glucose sensor based on a glassy carbon electrode modified with a nanocomposite made from nickel (II) hydroxide nanoplates and carbon nanofibers, Microchim. Acta. 181 (2014) 365–372.

[49] H. Tian, M. Jia, M. Zhang, J. Hu, Nonenzymatic glucose sensor based on nickel ion implanted-modified indium tin oxide electrode, Electrochim. Acta. 96 (2013) 285–290.

[50] J. Xu, F. Li, D. Wang, M.H. Nawaz, Q. An, D. Han, L. Niu, Co3O4 nanostructures on flexible carbon cloth for crystal plane effect of nonenzymatic electrocatalysis for glucose, Biosens. Bioelectron. 123 (2019) 25–29.

[51] C.-W. Kung, C.-Y. Lin, Y.-H. Lai, R. Vittal, K.-C. Ho, Cobalt oxide acicular nanorods with high sensitivity for the non-enzymatic detection of glucose, Biosens. Bioelectron. 27 (2011) 125–131.

[52] S. Park, H. Boo, T.D. Chung, Electrochemical non-enzymatic glucose sensors, Anal. Chim. Acta. 556 (2006) 46–57.

Figures

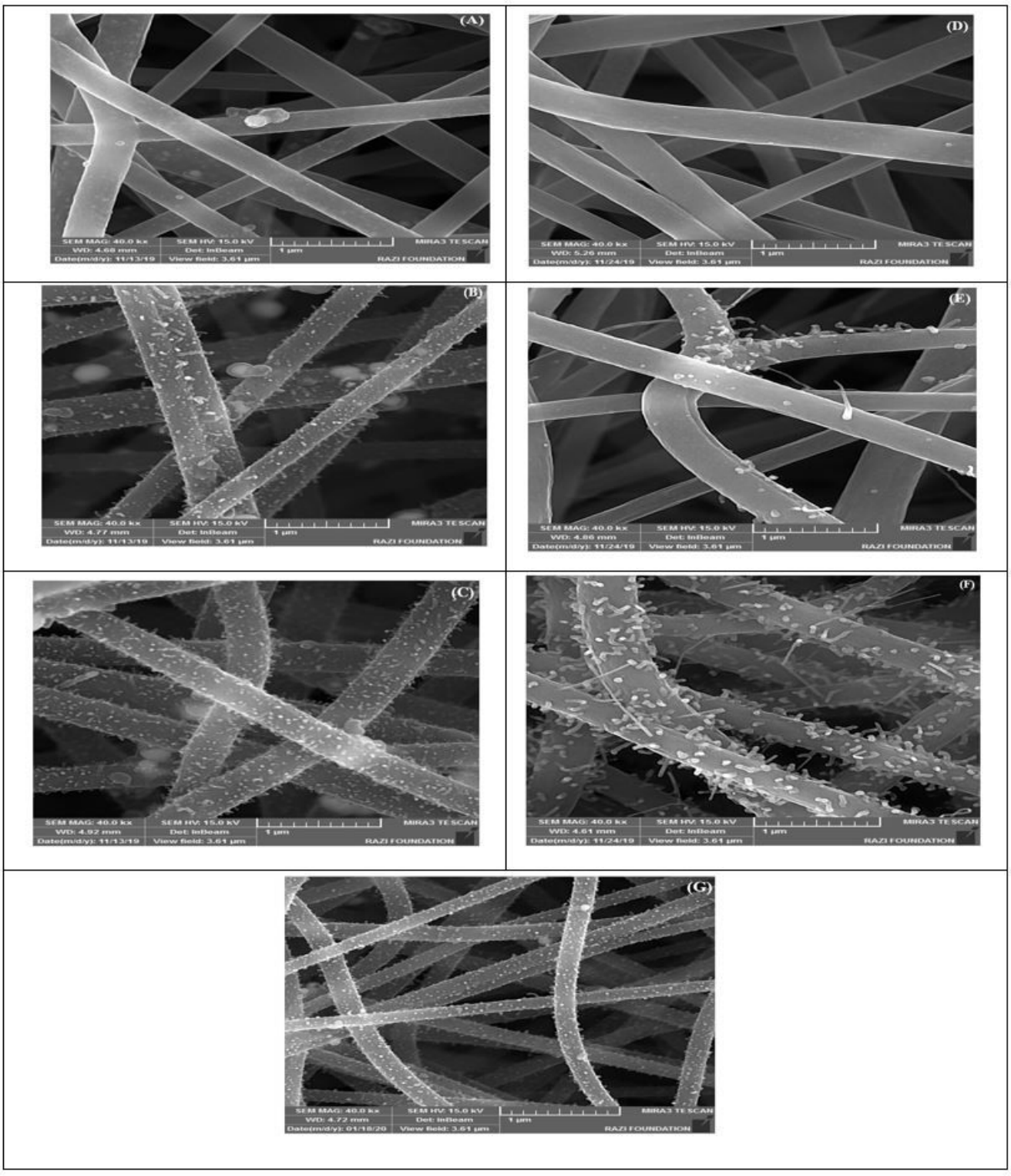

Figure 1

FESEM images of (A) 0.2 Ni/ ECNF-5h; (B) 0.35 Ni/ ECNF-5h; (C) 0.5 Ni/ ECNF-5h; (D) 0.2 Co/ ECNF-5h (E) 0.35 Co/ ECNF-5h; (F) 0.5 Co/ ECNF-5h; (G) Ni70Co30/ ECNF-5h.

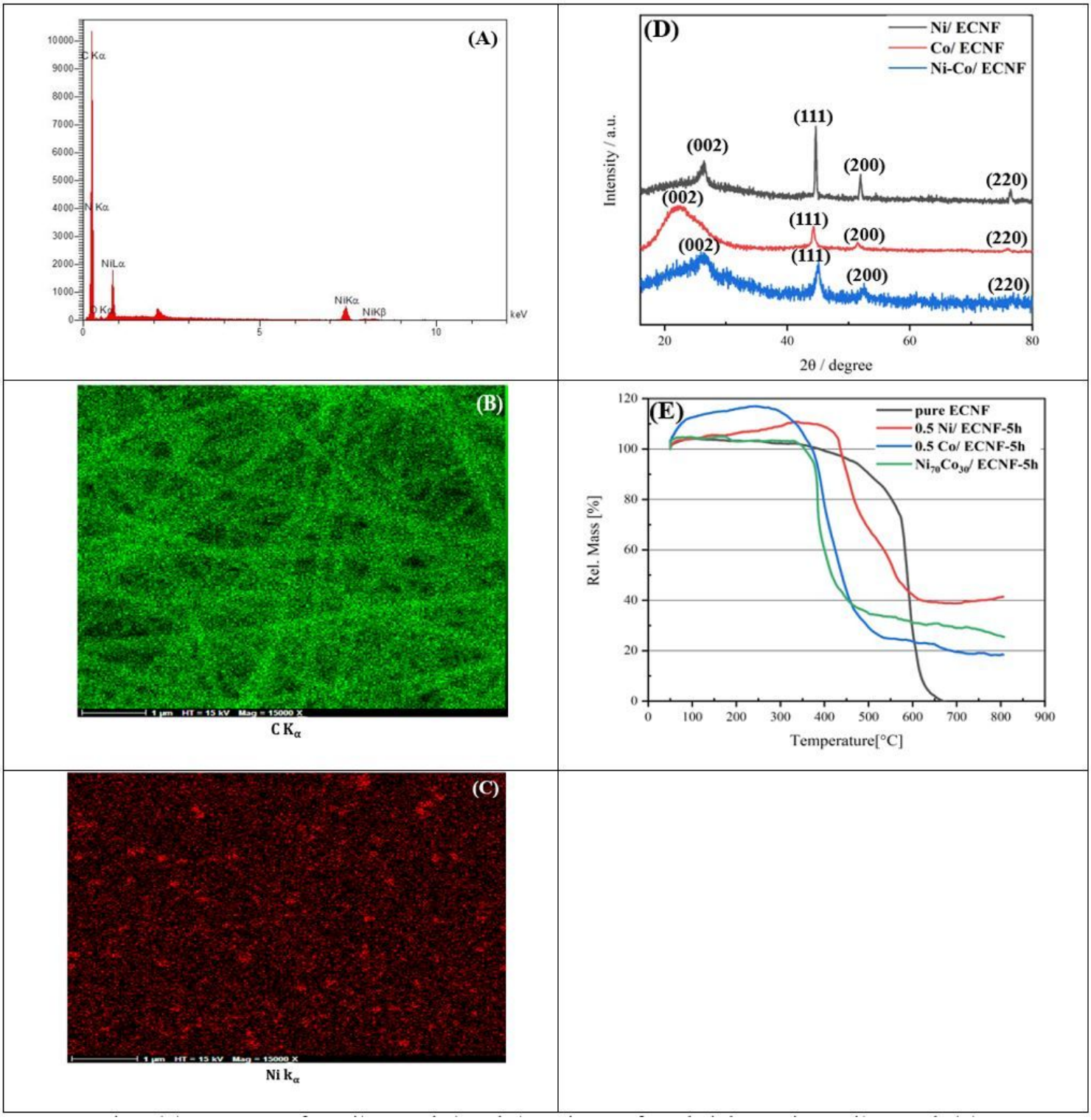

Figure 2

(A) EDX spectra of 0.5 Ni/ ECNF-5h. (B and C) map images of C and Ni elements in 0.5 Ni/ ECNF-5h. (D) XRD pattern of the Ni/ ECNF, Co/ ECNF and Ni-Co/ ECNF nanocomposites. (E) TGA curves for pure ECNF, and nanocomposites of 0.5 Ni/ ECNF-5h, 0.5 Co/ ECNF-5h and Ni70Co30/ ECNF-5h.

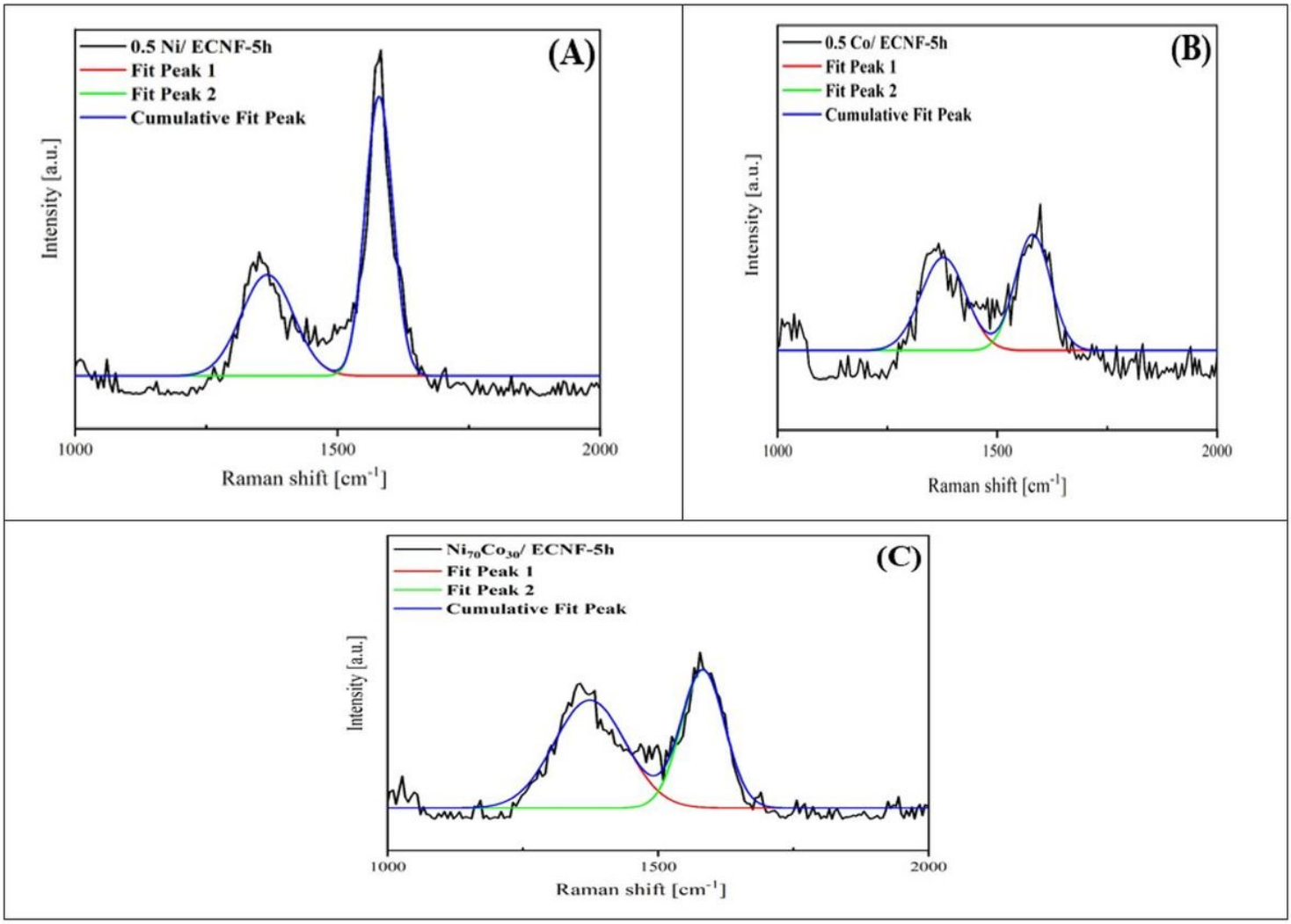

Figure 3

Raman spectra of (A) 0.5 Ni/ ECNF-5h, 0.5 Co/ ECNF-5h and Ni70Co30/ ECNF-5h nanocomposites.

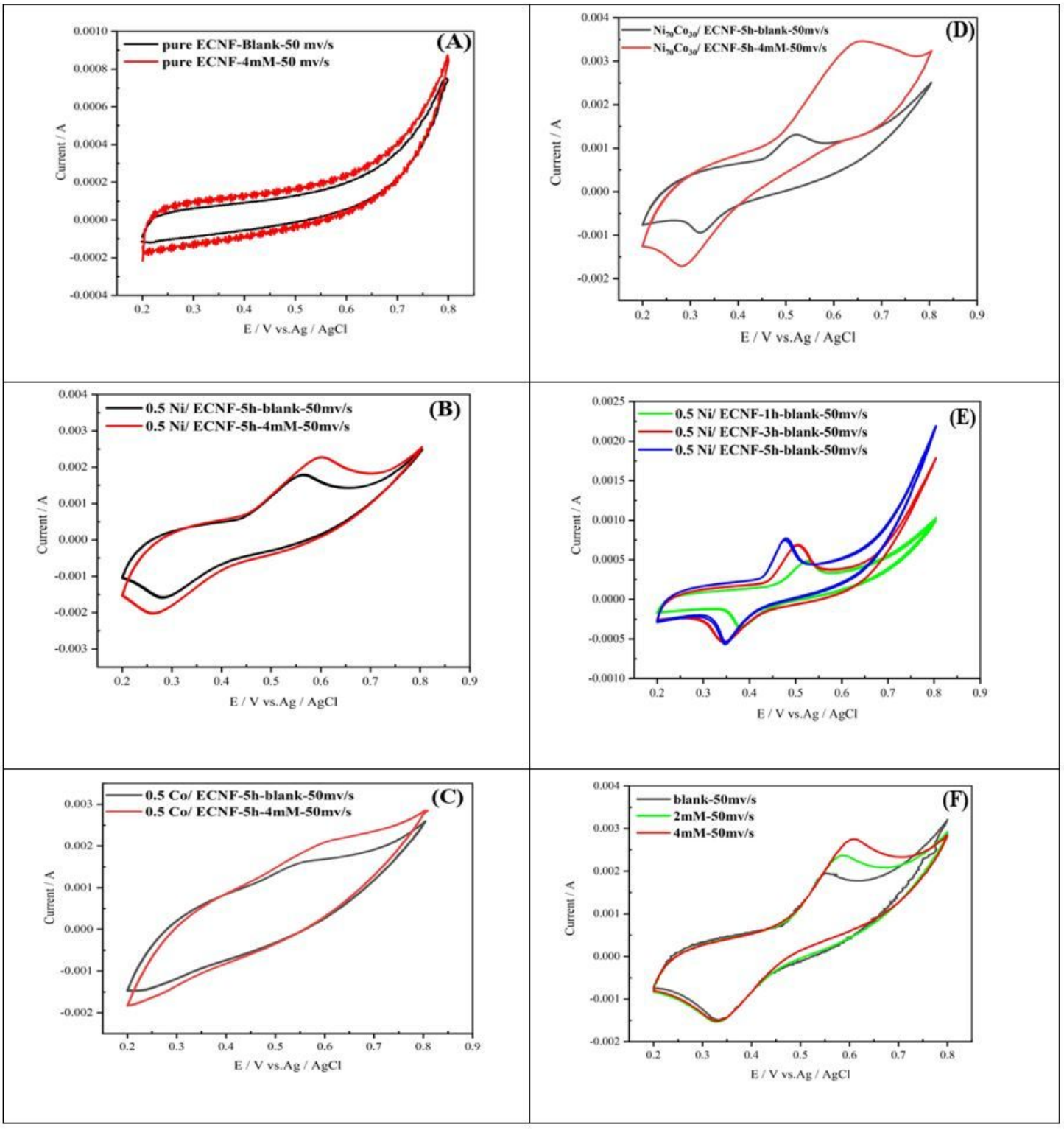

Figure 4

CVs of the (A) pure ECNF, (B) 0.5 Ni/ ECNF-5h, (C) 0.5 Co/ ECNF-5h (D) Ni70Co30/ ECNF-5h electrodes in the absence (dark line) and presence of 4.0 mM (red line) glucose, (E) Ni/ ECNF electrodes with different carbonization times in the absence of glucose, (F) effect of glucose concentration on the anodic peak current for 0.5 Ni/ ECNF-5h electrode in 0.1M NaOH solution at a scan rate of 50 mV s-1.

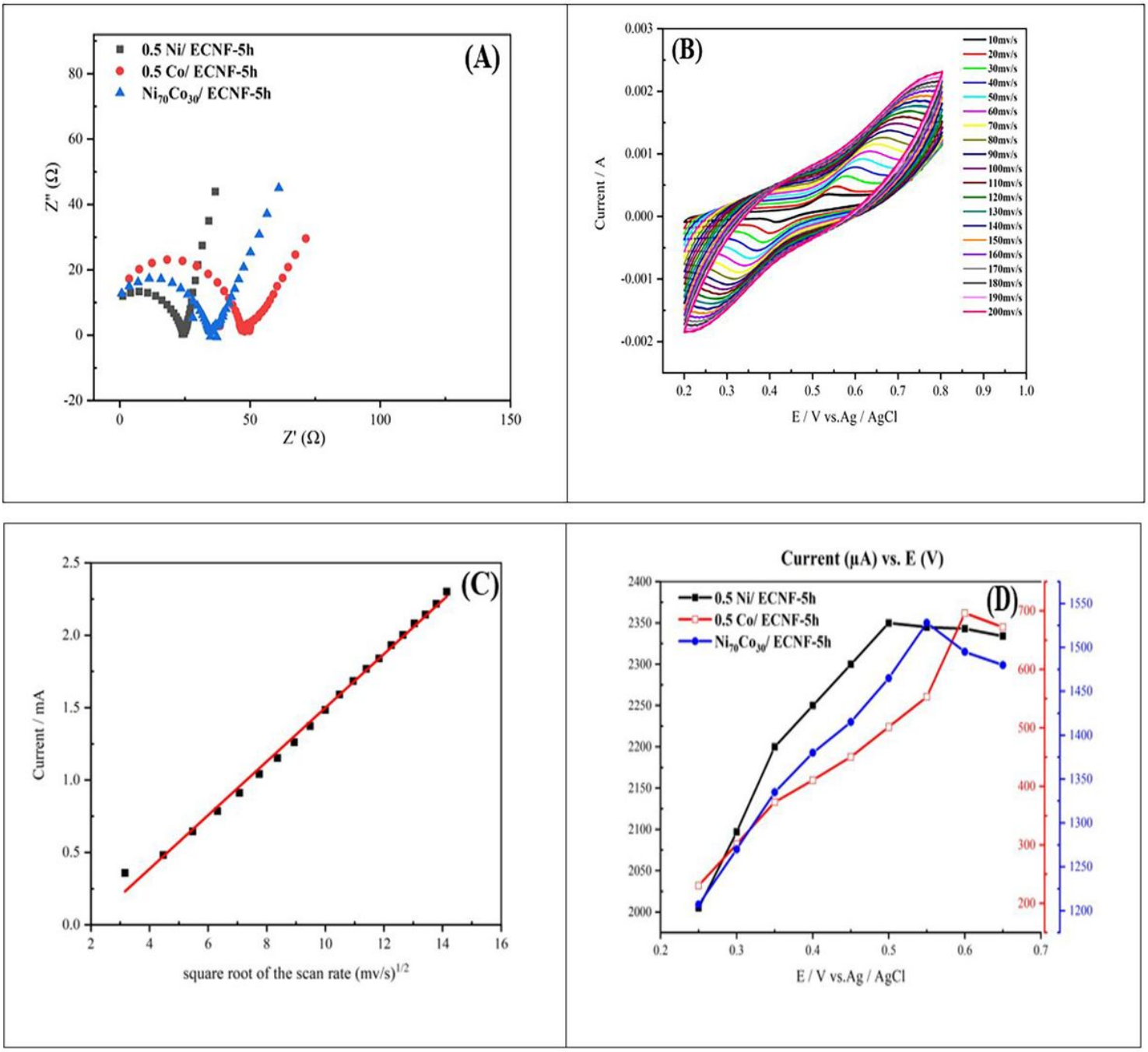

Figure 5

(A) Nyquist plots of 0.5 Ni/ ECNF-5h, 0.5 Co/ ECNF-5h and Ni70Co30/ ECNF-5h electrodes in 0.1 M KCl solution containing 5mM [Fe (CN)6]3-/4-. (B) CVs of 2.0 mM glucose at electrode with different scan rates ranging from 10 - 200 mV s-1 in 0.1 M NaOH, (C) the calibration curve of current vs square root of the scan rate, (D) Effects of applied potential on the amperometric response of the 0.5 Ni/ ECNF-5h, 0.5 Co/ ECNF-5h and Ni70Co30/ ECNF-5h biosensors to 4.0 mM glucose in 0.1 M NaOH.

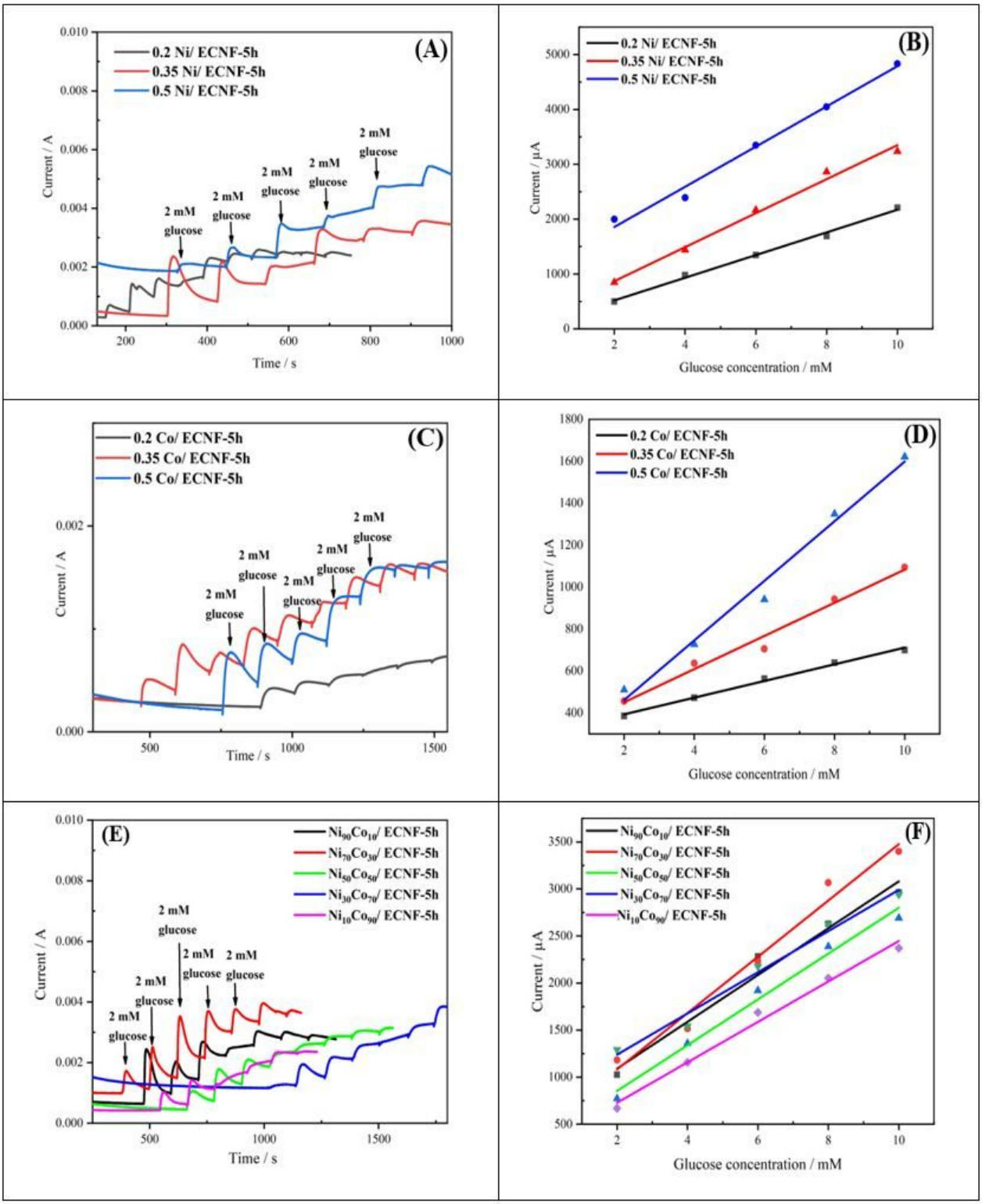

Figure 6

(A), (C) and (E) Current-time responses of the Ni/ ECNF, Co/ ECNF and Ni-Co/ ECNF biosensors upon successive addition of 2.0 mM glucose to 0.1 M NaOH solution at applied potential of +0.5, +0.6 and +0.55 V vs. Ag/AgCl. (B), (D) and (F) calibration curves of the Ni/ ECNF, Co/ ECNF and Ni-Co/ ECNF biosensors for glucose detection.

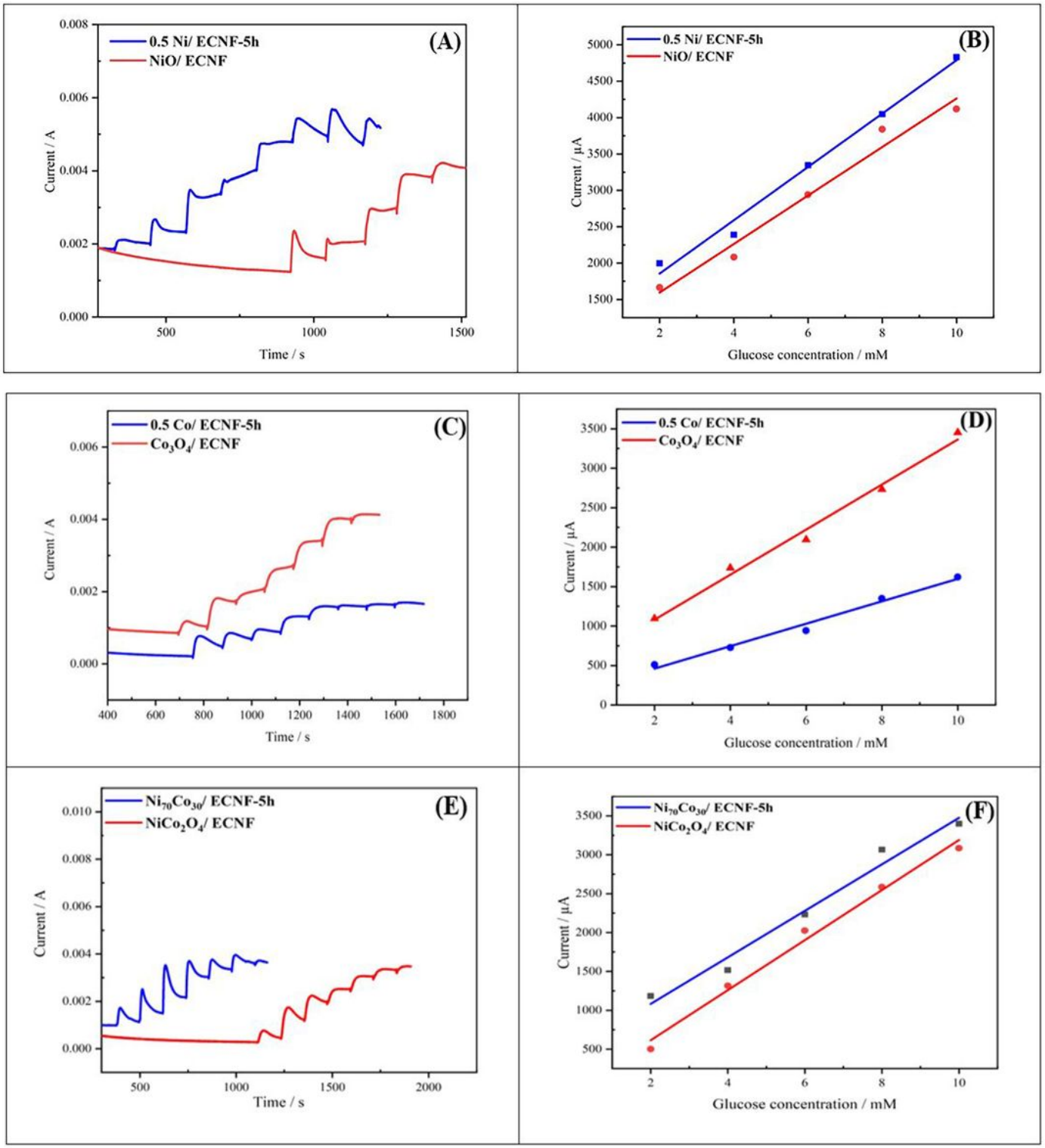

Figure 7

Comparison of Current-time responses of the (A) NiO/ ECNF with 0.5 Ni/ ECNF-5h biosensors, (C) Co3O4/ ECNF with Co/ ECNF-5h biosensors and (E) NiCo2O4/ ECNF with Ni70Co30/ ECNF-5h biosensors upon successive addition of 2.0 mM glucose to 0.1 M NaOH solution at applied potential of +0.5, +0.6 and +0.55 V vs. Ag/AgCl, respectively. (B), (D) and (F) calibration curves of the electrodes for glucose detection.

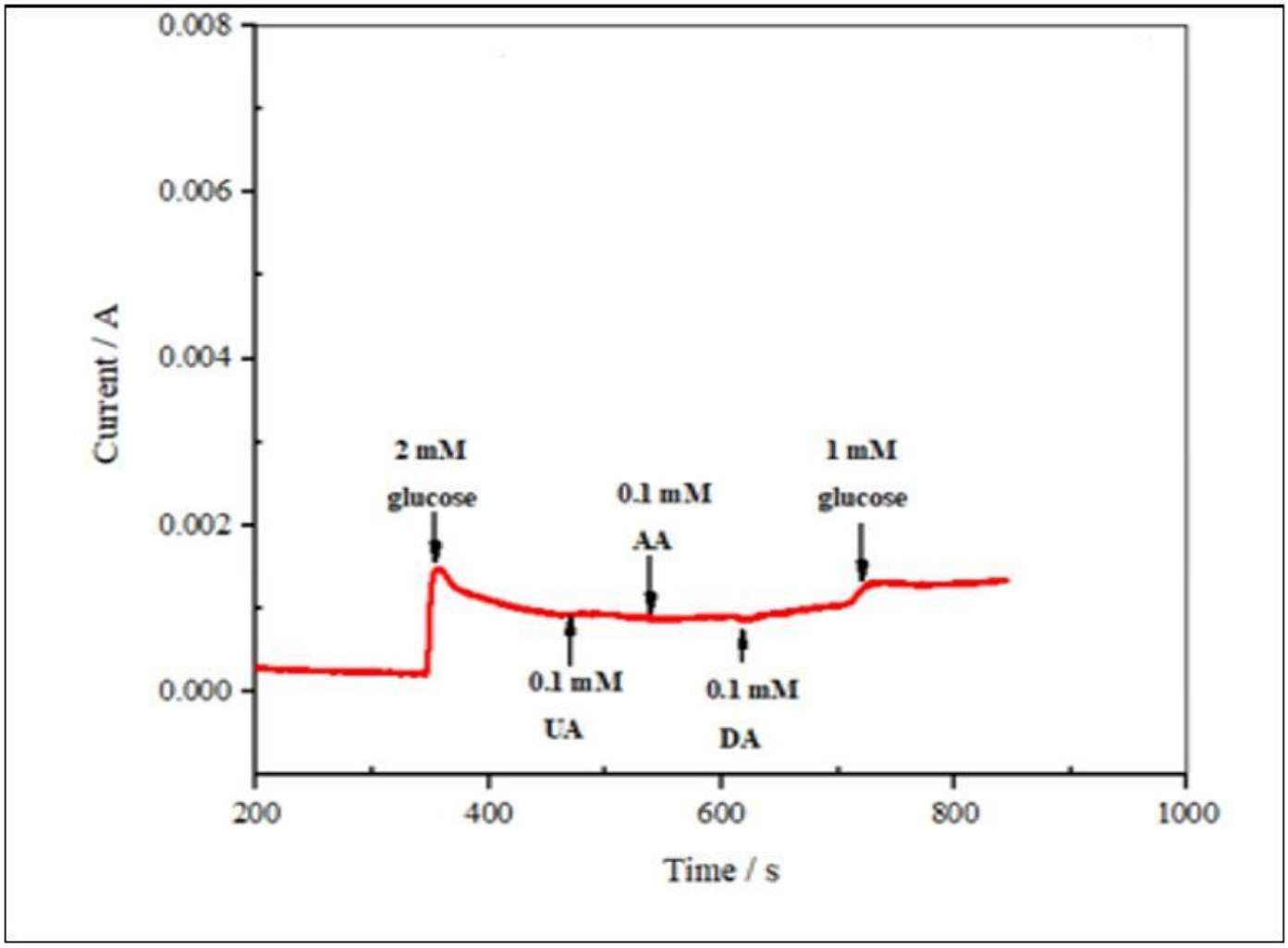

Figure 8

The amperometric response of electrode to successive injections of 1.0 and 2.0 mM glucose and 0.1 mM interferents of U.A., A.A., and DA in 0.1 M NaOH solution.

Supplementary Files

This is a list of supplementary files associated with this preprint. Click to download.

- SUPPLEMENTRY.docx